
Jaccard Metric Losses: Optimizing the Jaccard Index with Soft Labels

Zifu Wang¹ Matthew B. Blaschko¹

Abstract

IoU losses are surrogates that directly optimize the Jaccard index. In semantic segmentation, IoU losses are shown to perform better with respect to the Jaccard index measure than pixel-wise losses such as the cross-entropy loss. The most notable IoU losses are the soft Jaccard loss and the Lovasz-Softmax loss. However, these losses are incompatible with soft labels which are ubiquitous in machine learning. In this paper, we propose Jaccard metric losses (JMLs), which are variants of the soft Jaccard loss, and are compatible with soft labels. With JMLs, we study two of the most popular use cases of soft labels: label smoothing and knowledge distillation. With a variety of architectures, our experiments show significant improvements over the cross-entropy loss on three semantic segmentation datasets (Cityscapes, PASCAL VOC and DeepGlobe Land), and our simple approach outperforms state-of-the-art knowledge distillation methods by a large margin. Our source code is available at: <https://github.com/zifuwang/JDML>.

1. Introduction

The Jaccard index, or intersection-over-union (IoU) is commonly used in the evaluation of semantic segmentation models because it is scale invariant and a more adequate indicator for the perceptual quality of the model than pixel-wise accuracy (Eelbode et al., 2020). Statistical learning theory of empirical risk minimization states that we should optimize a loss function during training which we will also use for evaluation at testing (Vapnik, 1995). Therefore, directly optimizing IoU during training has been frequently considered in the literature (Nowozin, 2014; Rahman & Wang, 2016; Berman et al., 2018; Yu & Blaschko, 2018; Eelbode et al., 2020; Yu et al., 2021).

IoU only attains values when both predictions and ground-truth labels take discrete binary values. In other words, when

they both lie on the vertices of a p -dimensional hypercube $\{0, 1\}^p$. However, neural networks output soft probabilities that are in the interior of the hypercube $[0, 1]^p$. In order to extend the value of IoU from vertices to the whole hypercube, currently there are two popular approaches. The one is to relax set counting by norm functions, such as the soft Jaccard loss (SJL) (Nowozin, 2014; Rahman & Wang, 2016). The other is to compute the Lovasz extension of IoU, such as the Lovasz-Softmax loss (LSL) (Berman et al., 2018). These loss functions allow a plug-and-play use, and have greatly improved the performance of segmentation models over pixel-wise losses such as the cross-entropy loss (CE) and the focal loss (Lin et al., 2018). For example, Rakhlin et al. (Rakhlin et al., 2018) won the land cover segmentation task of DeepGlobe Challenge (Demir et al., 2018) using LSL. SJL and the soft Dice loss (Sudre et al., 2017) have also become the common practice of training neural networks for medical imaging (Eelbode et al., 2020; Isensee et al., 2021).

Soft labels are ubiquitous in machine learning. For instance, label smoothing (Szegedy et al., 2016) generates soft labels via a weighted average of one-hot hard labels and the uniform distribution over labels. In knowledge distillation (Hinton et al., 2015), class probabilities produced by a teacher network are used as soft labels to supervise a student model. Soft labels have been used in many state-of-the-art models and shown to improve both network’s accuracy and calibration (Müller et al., 2019). Nevertheless, as one interpolates IoU values for predictions from $\{0, 1\}^p$ to $[0, 1]^p$, the fact that labels can also be in $[0, 1]^p$ is overlooked. As a result, these IoU losses are incompatible with soft labels.

In this paper, firstly, we identify the limitation of various IoU losses and propose variants of SJL that we call Jaccard metric losses (JMLs) because they are a metric in $[0, 1]^p$. JMLs obtain the same value as SJL on hard labels, but are compatible with soft labels. Therefore, we can safely replace SJL with JMLs without affecting the performance on hard labels. Secondly, we study two of the most popular use cases of soft labels: label smoothing and knowledge distillation. We present boundary label smoothing (BLS) so as to integrate label smoothing into semantic segmentation. BLS not only improves the model’s performance but also leads to a better teacher. Under soft labels, we also investigate different ways to compute active classes which can

¹ESAT-PSI, KU Leuven, Leuven, Belgium. Correspondence to: Zifu Wang <zifu.wang@kuleuven.be>.

have a noticeable impact on the performance. We perform extensive experiments on Cityscapes (Cordts et al., 2016), PASCAL VOC (Everingham et al., 2009) and DeepGlobe Land (Demir et al., 2018). Our results show considerable improvements over the cross-entropy loss with various architectures, and our simple approach exceeds state-of-the-art knowledge distillation methods by a large margin.

2. Methods

2.1. Preliminaries

Given a segmentation output $\bar{x} \in \{1, \dots, C\}^p$ and a ground-truth $\bar{y} \in \{1, \dots, C\}^p$ where C is the number of classes, for each class c , we define the set of predictions as $x^c = \{\bar{x} = c\}$, the set of ground-truth as $y^c = \{\bar{y} = c\}$, the union as $u^c = x^c \cup y^c$, the intersection as $v^c = x^c \cap y^c$, the symmetric difference (the set of mispredictions) as $m^c = (x^c \setminus y^c) \cup (y^c \setminus x^c)$, and the Jaccard index as $\text{IoU}^c = |v^c|/|u^c|$. For multi-class segmentation, IoU^c are averaged across classes, yielding the mean IoU (mIoU). In the sequel, we will encode sets as binary vectors $x^c, y^c, u^c, v^c, m^c \in \{0, 1\}^p$ where p is the number of pixels, and denote $|x^c| = \sum_{i=1}^p x_i^c$ the cardinality of the corresponding set. For simplicity, we will drop the superscript on c in the following.

In order to optimize IoU in a continuous setting, we need smooth interpolations of this discrete score. In particular, we want to extend the IoU loss

$$\begin{aligned} \Delta_{\text{IoU}} : x \in \{0, 1\}^p, y \in \{0, 1\}^p \\ \mapsto 1 - \frac{|v|}{|u|} = \frac{|m|}{|y \cup m|} \end{aligned} \quad (1)$$

with $\bar{\Delta}_{\text{IoU}}$ so that it attains a value with any vector of predictions $\tilde{x} \in [0, 1]^p$. In what follows, when the context is clear, we will use x and \tilde{x} interchangeably.

The soft Jaccard loss (S JL) (Nowozin, 2014; Rahman & Wang, 2016) generalizes IoU by realizing that when $x, y \in \{0, 1\}^p$, $|v| = \langle x, y \rangle$ and $|u| = |x| + |y| - |v| = \|x\|_1 + \|y\|_1 - \langle x, y \rangle$. Therefore, S JL replaces the set notation with vector functions:

$$\begin{aligned} \bar{\Delta}_{\text{S JL}, L^1} : x \in [0, 1]^p, y \in \{0, 1\}^p \\ \mapsto 1 - \frac{\langle x, y \rangle}{\|x\|_1 + \|y\|_1 - \langle x, y \rangle}. \end{aligned} \quad (2)$$

The L^1 norm can be replaced with squared L^2 norm (Eelbode et al., 2020):

$$\begin{aligned} \bar{\Delta}_{\text{S JL}, L^2} : x \in [0, 1]^p, y \in \{0, 1\}^p \\ \mapsto 1 - \frac{\langle x, y \rangle}{\|x\|_2^2 + \|y\|_2^2 - \langle x, y \rangle}. \end{aligned} \quad (3)$$

2.2. The Limitation of IoU Losses

The main limitation of IoU losses is that they do not necessarily have desired properties when presented with soft labels. That is, when $y \in [0, 1]^p$. Let us first look at $\bar{\Delta}_{\text{S JL}, L^1}$ and consider a simple case with one pixel:

$$\bar{\Delta}_{\text{S JL}, L^1} = 1 - \frac{xy}{x + y - xy}. \quad (4)$$

One can easily verify that for any $y > 0$, $\bar{\Delta}_{\text{S JL}, L^1}$ is always minimized at $x = 1$ since $\bar{\Delta}_{\text{S JL}, L^1}$ is monotonically decreasing as a function of x . We therefore have that $\bar{\Delta}_{\text{S JL}, L^1}$ is in general not minimized when $x = y$, a basic desired property of a loss function. More analysis and experiments on real datasets are in the appendix.

$\bar{\Delta}_{\text{S JL}, L^2}$ does not have this issue since $\bar{\Delta}_{\text{S JL}, L^2} = 0 \Leftrightarrow \|x\|_2^2 + \|y\|_2^2 - 2\langle x, y \rangle = 0 \Leftrightarrow x = y$. However, the L^2 version is shown to give worse results than the L^1 counterpart (Eelbode et al., 2020), and it is rarely used in practice. For example, in SMP (Iakubovskii, 2019), a popular open source semantic segmentation project, only the L^1 version is implemented. Besides, the idea of replacing the set notation with L^1 norm has been widely adopted in many other works, including the soft Dice loss (Sudre et al., 2017), the soft Tversky loss (Salehi et al., 2017), the focal Tversky loss (Abraham & Khan, 2019) etc. As a result, they all fail to deal with soft labels for the same reason.

The Lovasz-Softmax loss (Berman et al., 2018), the Lovasz hinge loss (Yu & Blaschko, 2018) and the PixIoU loss (Yu et al., 2021) all cannot handle soft labels, because they rely on the Lovasz extension which is not well defined when $y \in (0, 1)^p$. We provide more details of the Lovasz extension in the appendix. Automatically searched loss functions such as Auto Seg-Loss (Li et al., 2021) and AutoLoss-Zero (Li et al., 2022) also cannot deal with soft labels because their search space is defined only for integral labels.

2.3. Jaccard Metric Losses

Ideally, we want to extend Δ_{IoU} with a loss function $\bar{\Delta} : [0, 1]^p \times [0, 1]^p \rightarrow [0, 1]$ that satisfies the following properties:

- (a) $\forall x, y \in [0, 1]^p, x = y \Leftrightarrow \bar{\Delta} = 0$.
- (b) $\forall x \in [0, 1]^p, y \in \{0, 1\}^p, \bar{\Delta} = \bar{\Delta}_{\text{S JL}, L^1}$ or $\bar{\Delta}_{\text{L SL}}$.

Property (a) guarantees that it is compatible with soft labels. Property (b) indicates that when we only have hard labels, we can safely replace S JL or L SL with this loss function and the result will remain identical.

It is a well-known result that Δ_{IoU} is a metric in $\{0, 1\}^p$ (Kosub, 2019). Recall the definition of a metric in $[0, 1]^p$:

Definition 2.1 (Metric). A mapping $f : [0, 1]^p \times [0, 1]^p \rightarrow \mathbb{R}$ is called a metric if it satisfies the following conditions for all $a, b, c \in [0, 1]^p$:

- (i) $f(a, a) = 0$.
- (ii) (Positivity). If $a \neq b$, then $f(a, b) > 0$.
- (iii) (Symmetry). $f(a, b) = f(b, a)$.
- (iv) (Triangle inequality). $f(a, c) \leq f(a, b) + f(b, c)$.

It is nice to have to a loss function $\bar{\Delta}$ being a metric. Conditions (i) and (ii) jointly imply property (a), and therefore $\bar{\Delta}$ would be compatible with soft labels. The triangle inequality is also instructive. Applying it to knowledge distillation:

$$\bar{\Delta}(S, L) \leq \bar{\Delta}(S, T) + \bar{\Delta}(T, L), \quad (5)$$

where S the student, T the teacher and L the ground-truth label. In knowledge distillation, we first train a teacher with the ground-truth label and then minimize the loss between the teacher and the student. Eq. (5) indicates that if we follow this procedure, which is equivalent to minimizing the right hand side, the upper bound on the student’s loss with respect to the ground-truth label will also be minimized.

We leave a generalization of the Lovasz extension of Δ_{IoU} to the case that $x, y \in [0, 1]^p$ as an open problem. In this paper, we focus on re-deriving SJL. In particular, we can rewrite the union and the intersection as a function of the set difference:

$$|v| = \frac{1}{2}(|x| + |y| - |m|), \quad (6)$$

$$|u| = |v| + |m|. \quad (7)$$

Note that $|m| = \|x - y\|_1$. Combining these yields:

$$|v| = \|x \odot y\|_1 \quad (8)$$

$$= \frac{1}{2}(\|x + y\|_1 - \|x - y\|_1), \quad (9)$$

$$|u| = \|x \odot y\|_1 + \|x - y\|_1 \quad (10)$$

$$= \frac{1}{2}(\|x\|_1 + \|y\|_1 + \|x - y\|_1), \quad (11)$$

where the equalities hold when $x, y \in \{0, 1\}^p$.

After eliminating erroneous combinations that have the same issue as SJL, we are left with two candidates $\bar{\Delta}_{JML,1}, \bar{\Delta}_{JML,2} : [0, 1]^p \times [0, 1]^p \rightarrow [0, 1]$ that are defined as:

$$\bar{\Delta}_{JML,1} = 1 - \frac{\|x + y\|_1 - \|x - y\|_1}{\|x + y\|_1 + \|x - y\|_1}, \quad (12)$$

$$\bar{\Delta}_{JML,2} = 1 - \frac{\|x \odot y\|_1}{\|x \odot y\|_1 + \|x - y\|_1}. \quad (13)$$

We can show that both $\bar{\Delta}_{JML,1}$ and $\bar{\Delta}_{JML,2}$ are metrics in $[0, 1]^p$, and we call them Jaccard metric losses (JMLs).

Theorem 2.2. Both $\bar{\Delta}_{JML,1}$ and $\bar{\Delta}_{JML,2}$ are metrics in $[0, 1]^p$. Neither $\bar{\Delta}_{SJL,L^1}$ nor $\bar{\Delta}_{SJL,L^2}$ is a metric in $[0, 1]^p$.

Besides, when we only have hard labels, we can use them interchangeably.

Theorem 2.3. $\forall x \in [0, 1]^p, y \in \{0, 1\}^p$ and $x \in \{0, 1\}^p, y \in [0, 1]^p, \bar{\Delta}_{SJL,L^1} = \bar{\Delta}_{JML,1} = \bar{\Delta}_{JML,2}$. $\exists x, y \in [0, 1]^p, \bar{\Delta}_{SJL,L^1} \neq \bar{\Delta}_{JML,1} \neq \bar{\Delta}_{JML,2}$.

Proofs can be found in the appendix. Now we have two loss functions that are both metrics but attain different values when $x, y \in [0, 1]^p$. Which one should we choose? We discuss their differences in the appendix. Theoretically and empirically, we find $\bar{\Delta}_{JML,1}$ is slightly favored over $\bar{\Delta}_{JML,2}$. In our experiments, we use $\bar{\Delta}_{JML,1}$ as a default.

2.4. Use Cases

Soft labels have a wide range of applications. In this paper, we study two of the most popular use cases: label smoothing and knowledge distillation.

2.4.1. LABEL SMOOTHING

In label smoothing (LS) (Szegedy et al., 2016), the one-hot encoding is mixed with the uniform distribution with a parameter ϵ , resulting in soft labels SL^ϵ . In JML-LS, a model M is optimized with the following loss:

$$\mathcal{L}_{JML-LS} = \lambda \mathcal{L}_{CE,LS} + (1 - \lambda) \mathcal{L}_{JML,LS} \quad (14)$$

such that $\mathcal{L}_{CE,LS} = CE(M, SL^\epsilon)$ and $\mathcal{L}_{JML,LS} = JML(M, SL^\epsilon)$.

LS ignores spatial dependencies. If we view semantic segmentation as a pixel-wise classification task and apply LS to every pixel in the image, we may overly smooth regions that the network is already very accurate. In semantic segmentation, the model often suffers at the boundary region. Therefore, we propose boundary label smoothing (BLS) that only smooths labels near the boundary. Specifically, for every pixel i , we look at its $k \times k$ neighbor N_i . We define a pixel i as a boundary pixel if there exists a pixel $j \in N_i$ so that their ground-truth labels are different: $y_i \neq y_j$. This can be easily computed by applying a max pooling layer over the one-hot encoding.

2.4.2. KNOWLEDGE DISTILLATION

In knowledge distillation (KD) (Hinton et al., 2015), besides the ground-truth label L , a student model is trained to together minimize the discrepancy to a teacher network T :

$$\mathcal{L}_{CE,KD} = \mu \mathcal{L}_{CE,L} + (1 - \mu) \mathcal{L}_{CE,T} \quad (15)$$

where $\mathcal{L}_{\text{CE}, L} = \text{CE}(S, L)$ and $\mathcal{L}_{\text{CE}, T} = \text{CE}(S, T)$. In JML-KD, we add additional supervision from JML:

$$\mathcal{L}_{\text{JML}, \text{KD}} = \nu \mathcal{L}_{\text{JML}, L} + (1 - \nu) \mathcal{L}_{\text{JML}, T} \quad (16)$$

where $\mathcal{L}_{\text{JML}, L} = \text{JML}(S, L)$ and $\mathcal{L}_{\text{JML}, T} = \text{JML}(S, T)$. Combining these, we have

$$\mathcal{L}_{\text{JML-KD}} = \lambda \mathcal{L}_{\text{CE}, \text{KD}} + (1 - \lambda) \mathcal{L}_{\text{JML}, \text{KD}}. \quad (17)$$

2.4.3. ACTIVE CLASSES

It is vital to determine which classes contribute to the loss value at each iteration. With hard labels, if the network wrongly predicts a single pixel to a class c that is absent in the current batch, the loss value will change from 1 to 0. Thus, LSL suggests to compute the loss only over classes that are present in the current batch so that the loss is more stable to single predictions in absent classes. In the literature (Rahman & Wang, 2016) and popular open-source libraries such as SMP (Iakubovskii, 2019), SJL is usually implemented to compute the loss with all classes. We speculate this is because SJL is often used in medical imaging where the number of classes is small and therefore most classes will appear in the same batch.

With soft labels, a similar issue exists. We show an example with an extremely small soft label $y = 0.05$ in Figure 1. The loss becomes excessively steep around the target but flattens out when the prediction is close to 1. This is intrinsically a problem by the definition of IoU - it is defined to be 0 when there is no ground-truth. Moreover, since each class is weighted equally, if we compute the loss over all classes, the model may be distracted by irrelevant classes. For example, in KD, a teacher network may contain noisy and useless predictions over unimportant classes. What if we only use present classes? For soft labels, present classes in the current batch are those when we take argmax in the class dimension. Nevertheless, the power of BLS and KD depend on these non-argmax classes. Specifically, in KD, it is critical for the student to utilize information of these non-target classes to learn class relationships from the teacher (Tang et al., 2020; Zhao et al., 2022). Given this insight, we propose to skip classes that have low confidence. Hence, the model will focus on the most relevant classes. Different variants are summarized in Figure 4 (in the appendix). In particular, in mode “label”, we ignore classes that the soft label, e.g. teacher’s confidence, is low. In mode “prob”, we skip classes such that the model itself is not confident. In mode “both”, we take both into account.

3. Experiments

3.1. Implementation Details

We adopt Pytorch Image Models (timm) (Wightman, 2019), which provides implementations and ImageNet (Deng et al.,

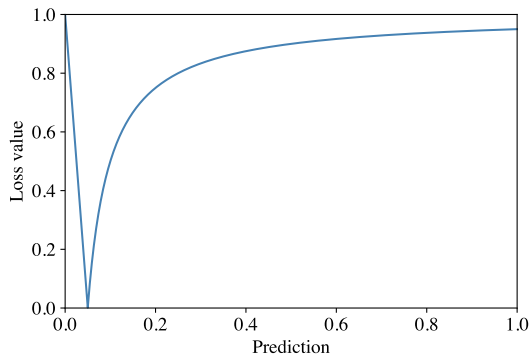


Figure 1. Loss value vs. prediction with $y = 0.05$.

2009) pre-trained weights for various backbones. In our experiments, backbones include ResNet-101, ResNet-50, ResNet-18 (He et al., 2016) and MobileNetV2 (Sandler et al., 2018). Models consist of DeepLabV3 (Chen et al., 2017), PSPNet (Zhao et al., 2017) and UNet (Ronneberger et al., 2015).

We follow training details in (Yang et al., 2022b; Huang et al., 2022b;a) except that we use a smaller batch size of 8. In particular, we use SGD with a momentum of 0.9 and an initial learning rate of 0.01. The learning rate is decayed by $(1 - \frac{\text{iter}}{\text{total iters}})^{0.9}$ and the number of iterations¹ is 40K for Cityscapes (Cordts et al., 2016) and PASCAL VOC (Everingham et al., 2009), 10K for DeepGlobe Land (Demir et al., 2018). The crop size is 512×1024 for Cityscapes (Cordts et al., 2016), 512×512 for PASCAL VOC (Everingham et al., 2009) and DeepGlobe Land (Demir et al., 2018). For JML experiments, we set $\mu = \nu = 0.5$ and $\lambda = 0.25$.

For a comprehensive comparison, we present both overall pixel-wise accuracy (Acc) and mean intersection-over-union (mIoU). To show the effect of our methods on calibration, we report the expected calibration error (ECE) (Guo et al., 2017) and ECE that is computed only over the boundary region, denoted as BECE.

For Cityscapes and PASCAL VOC, we repeat the experiments 3 times and report the performance on the validation set. For DeepGlobe Land, since there is no official train/validation split, we use 5-fold cross-validation. All results are in the format of mean \pm standard deviation.

3.2. Main Results

The main results are shown in Tables 1, 2 and 3. Compared with CE, JML can significantly increase a model’s mIoU. The improvement is usually more than 2% on Cityscapes

¹For the ease of implementation, our training script is per-epoch based. The number of iterations is very close, but not identical to 10K/40K.

Jaccard Metric Losses: Optimizing the Jaccard Index with Soft Labels

Table 1. Results on Cityscapes. M0: DeepLabV3-ResNet101, M1: DeepLabV3-ResNet50, M2: DeepLabV3-ResNet18, M3: DeepLabV3-MobileNetV2, M4: PSPNet-ResNet18. Best results within CE and JML groups are highlighted in red and green, respectively. Best results across CE and JML groups are underscored.

Model	Metric	CE	CE-BLS	CE-KD	JML	JML-BLS	JML-KD
M0	Acc (%)	96.10 ± 0.02	96.11 ± 0.03	-	96.10 ± 0.04	96.25 ± 0.03	-
	mIoU (%)	78.67 ± 0.32	78.70 ± 0.26	-	80.29 ± 0.17	80.66 ± 0.24	-
	ECE (%)	0.76 ± 0.05	0.97 ± 0.04	-	2.74 ± 0.03	2.09 ± 0.02	-
	BECE (%)	16.14 ± 0.22	11.59 ± 0.12	-	30.78 ± 0.19	21.20 ± 0.07	-
M1	Acc (%)	95.77 ± 0.08	95.83 ± 0.08	-	95.93 ± 0.04	96.05 ± 0.02	-
	mIoU (%)	76.45 ± 0.68	77.02 ± 0.82	-	78.68 ± 0.42	79.10 ± 0.35	-
	ECE (%)	0.62 ± 0.02	1.00 ± 0.03	-	2.84 ± 0.02	2.18 ± 0.01	-
	BECE (%)	16.23 ± 0.16	11.67 ± 0.18	-	31.12 ± 0.10	20.51 ± 0.12	-
M2	Acc (%)	95.28 ± 0.02	95.31 ± 0.05	95.40 ± 0.04	95.46 ± 0.04	95.49 ± 0.05	95.59 ± 0.02
	mIoU (%)	72.88 ± 0.44	73.14 ± 0.12	74.09 ± 0.28	75.55 ± 0.13	76.26 ± 0.17	76.68 ± 0.33
	ECE (%)	0.68 ± 0.06	0.88 ± 0.01	0.98 ± 0.03	3.07 ± 0.01	2.49 ± 0.05	2.47 ± 0.01
	BECE (%)	17.28 ± 0.19	13.25 ± 0.16	16.26 ± 0.18	32.10 ± 0.08	22.66 ± 0.10	22.57 ± 0.17
M3	Acc (%)	95.24 ± 0.01	95.28 ± 0.03	95.30 ± 0.04	95.45 ± 0.02	95.51 ± 0.04	95.56 ± 0.03
	mIoU (%)	72.19 ± 0.12	72.54 ± 0.26	72.88 ± 0.15	75.32 ± 0.42	75.81 ± 0.14	75.94 ± 0.24
	ECE (%)	0.69 ± 0.05	0.96 ± 0.03	0.99 ± 0.04	3.09 ± 0.02	2.43 ± 0.04	2.50 ± 0.03
	BECE (%)	17.64 ± 0.15	13.14 ± 0.20	16.55 ± 0.10	32.08 ± 0.29	21.61 ± 0.09	22.57 ± 0.04
M4	Acc (%)	95.13 ± 0.05	95.07 ± 0.03	95.14 ± 0.02	95.25 ± 0.02	95.30 ± 0.02	95.39 ± 0.01
	mIoU (%)	72.61 ± 0.34	72.43 ± 0.05	72.79 ± 0.15	74.96 ± 0.16	75.31 ± 0.13	75.75 ± 0.31
	ECE (%)	0.68 ± 0.07	0.97 ± 0.01	1.08 ± 0.05	3.17 ± 0.01	2.44 ± 0.02	2.52 ± 0.01
	BECE (%)	17.54 ± 0.24	13.61 ± 0.20	16.96 ± 0.21	32.65 ± 0.07	22.30 ± 0.15	23.17 ± 0.08

Table 2. Results on PASCAL VOC. M0: DeepLabV3-ResNet101, M1: DeepLabV3-ResNet50, M2: DeepLabV3-ResNet18, M3: DeepLabV3-MobileNetV2, M4: PSPNet-ResNet18. Best results within CE and JML groups are highlighted in red and green, respectively. Best results across CE and JML groups are underscored.

Model	Metric	CE	CE-BLS	CE-KD	JML	JML-BLS	JML-KD
M0	Acc (%)	94.68 ± 0.02	94.75 ± 0.05	-	94.97 ± 0.13	95.34 ± 0.08	-
	mIoU (%)	78.39 ± 0.09	78.87 ± 0.44	-	80.26 ± 0.45	81.52 ± 0.41	-
	ECE (%)	2.33 ± 0.03	2.01 ± 0.04	-	3.97 ± 0.10	3.20 ± 0.04	-
	BECE (%)	20.54 ± 0.12	17.25 ± 0.14	-	32.70 ± 0.09	22.30 ± 0.02	-
M1	Acc (%)	94.23 ± 0.05	94.28 ± 0.06	-	94.60 ± 0.02	94.87 ± 0.02	-
	mIoU (%)	76.93 ± 0.32	77.23 ± 0.18	-	78.97 ± 0.12	79.76 ± 0.15	-
	ECE (%)	2.05 ± 0.03	1.77 ± 0.08	-	4.19 ± 0.02	3.25 ± 0.02	-
	BECE (%)	20.95 ± 0.13	17.30 ± 0.15	-	33.07 ± 0.10	20.41 ± 0.01	-
M2	Acc (%)	92.96 ± 0.05	93.17 ± 0.09	93.13 ± 0.07	93.28 ± 0.14	93.72 ± 0.05	93.75 ± 0.05
	mIoU (%)	72.47 ± 0.33	72.99 ± 0.42	72.96 ± 0.30	74.42 ± 0.52	75.60 ± 0.24	75.89 ± 0.29
	ECE (%)	1.83 ± 0.12	1.26 ± 0.08	1.68 ± 0.05	4.92 ± 0.14	3.79 ± 0.03	3.94 ± 0.07
	BECE (%)	21.83 ± 0.29	17.87 ± 0.08	19.42 ± 0.04	34.35 ± 0.09	22.45 ± 0.08	22.15 ± 0.19
M3	Acc (%)	92.47 ± 0.12	92.45 ± 0.02	92.54 ± 0.04	92.74 ± 0.07	93.13 ± 0.11	93.21 ± 0.01
	mIoU (%)	70.14 ± 0.54	70.36 ± 0.27	70.54 ± 0.10	72.35 ± 0.32	73.25 ± 0.18	73.55 ± 0.27
	ECE (%)	1.92 ± 0.14	1.46 ± 0.09	1.78 ± 0.03	5.19 ± 0.05	4.14 ± 0.08	4.24 ± 0.01
	BECE (%)	22.65 ± 0.34	19.62 ± 0.45	20.62 ± 0.34	35.10 ± 0.17	23.38 ± 0.19	23.09 ± 0.11
M4	Acc (%)	92.93 ± 0.12	93.09 ± 0.09	93.13 ± 0.18	93.20 ± 0.08	93.65 ± 0.04	93.60 ± 0.10
	mIoU (%)	72.10 ± 0.55	72.76 ± 0.52	72.84 ± 0.57	74.20 ± 0.24	75.04 ± 0.22	74.93 ± 0.36
	ECE (%)	1.92 ± 0.22	1.40 ± 0.16	1.81 ± 0.16	4.76 ± 0.04	3.70 ± 0.01	3.99 ± 0.07
	BECE (%)	22.39 ± 0.39	18.95 ± 0.12	20.55 ± 0.47	34.72 ± 0.06	23.45 ± 0.20	23.53 ± 0.37

Table 3. Results on DeepGlobe Land. M5: UNet-ResNet50, M6: UNet-ResNet18, M7: UNet-MobileNetV2. Best results within CE and JML groups are highlighted in red and green, respectively. Best results across CE and JML groups are underscored.

Model	Metric	CE	CE-BLS	CE-KD	JML	JML-BLS	JML-KD
M5	Acc (%)	86.89 ± 0.87	<u>86.95 ± 0.99</u>	-	86.59 ± 0.84	<u>86.87 ± 0.79</u>	-
	mIoU (%)	68.80 ± 1.07	<u>68.86 ± 0.81</u>	-	69.29 ± 0.87	<u>69.73 ± 0.89</u>	-
	ECE (%)	1.77 ± 0.52	<u>1.68 ± 0.46</u>	-	12.34 ± 1.18	<u>11.68 ± 1.55</u>	-
	BECE (%)	21.93 ± 0.83	<u>21.90 ± 1.21</u>	-	40.97 ± 0.90	<u>39.22 ± 1.06</u>	-
M6	Acc (%)	84.99 ± 1.15	85.28 ± 0.97	<u>85.51 ± 0.76</u>	85.46 ± 0.56	85.53 ± 0.59	<u>85.78 ± 0.66</u>
	mIoU (%)	64.38 ± 1.50	64.93 ± 0.79	<u>66.40 ± 0.86</u>	66.95 ± 0.25	66.87 ± 0.30	<u>67.62 ± 0.27</u>
	ECE (%)	<u>1.05 ± 0.48</u>	1.47 ± 0.60	1.38 ± 0.61	10.32 ± 0.862	<u>9.15 ± 0.79</u>	9.83 ± 1.53
	BECE (%)	23.23 ± 0.54	<u>22.32 ± 0.75</u>	25.23 ± 0.75	40.17 ± 0.48	<u>38.13 ± 0.63</u>	39.24 ± 0.94
M7	Acc (%)	84.93 ± 1.11	84.92 ± 1.22	<u>85.64 ± 1.02</u>	85.54 ± 0.88	85.82 ± 0.66	<u>85.90 ± 0.73</u>
	mIoU (%)	64.38 ± 1.21	64.03 ± 1.73	<u>66.29 ± 1.39</u>	66.63 ± 0.73	67.04 ± 0.77	<u>67.46 ± 0.99</u>
	ECE (%)	1.64 ± 0.75	2.04 ± 0.74	<u>1.52 ± 0.34</u>	10.22 ± 1.37	10.01 ± 0.92	<u>9.67 ± 0.86</u>
	BECE (%)	21.15 ± 0.89	<u>20.26 ± 0.74</u>	24.76 ± 1.17	40.40 ± 0.89	39.28 ± 0.27	<u>38.82 ± 1.12</u>

Table 4. Comparing with state-of-the-art KD methods on Cityscapes and PASCAL VOC, including SKD (Liu et al., 2019), IFVD (Wang et al., 2020), CWD (Shu et al., 2021), CIRKD (Yang et al., 2022b), MasKD (Huang et al., 2022b), DIST (Huang et al., 2022a). Results of our method are mean±standard deviation (maximum over 3 runs). All results are mIoU (%). JML-KD*: we increase the batch size to 16 in Cityscapes experiments to match training details in CIRKD (Yang et al., 2022b) and DIST (Huang et al., 2022a).

Dataset	Model	SKD	IFVD	CWD	CIRKD	MasKD	DIST	JML-KD*
CS	DL3-R18	75.42	75.59	75.55	76.38	77.00	77.10	77.91 ± 0.16(78.14)
	DL3-MB2	73.82	73.50	74.66	75.42	75.26	-	77.53 ± 0.20(77.78)
	PSP-R18	73.29	73.71	74.36	74.73	75.34	76.31	77.33 ± 0.38(77.75)
VOC	DL3-R18	73.51	73.85	74.02	74.50	-	-	75.89 ± 0.29(76.25)
	PSP-R18	74.07	73.54	73.99	74.78	-	-	74.93 ± 0.36(75.36)

and PASCAL. Besides, it can also increase a model’s overall pixel accuracy. One might argue that the improvement on DeepGlobe Land is small compared with the standard deviation. We point out that the large variance not only comes from the methods themselves, but also the data splits. We report the results of BLS and KD on 5 folds of DeepGlobe Land in Table 9 (in the appendix) and it can be seen that JML provides consistent improvements over CE.

For KD experiments, the teacher is DL3-R50 trained with JML-BLS. We can see that both JML-BLS and JML-KD reliably improve the model’s accuracy. We find BLS is more effective on PASCAL VOC where the boundary condition is less complex. When it becomes more intricate, such as in Cityscapes, KD as learned label smoothing (Yuan et al., 2020) usually outperforms BLS. We also find that models trained with JML benefit more from soft labels. For example, the improvements of mIoU for DL3-R101 on PASCAL VOC are 0.48% (78.87% – 78.39%, CE vs. CE-BLS) and 1.25% (81.51% – 80.26%, JML vs. JML-BLS), respectively. We adopt training recipes that are heavily optimized for CE, and this might explain why JML needs stronger regularization.

As shown in Table 4, without bells and whistles, our simple approach that only utilizes soft labels greatly exceeds state-of-the-art KD methods. Indeed, the model that is trained only with hard labels in JML already achieves a comparable

result as some of these methods. For example, DL3-R18 on PASCAL VOC achieves $74.42 \pm 0.52\%$ mIoU while CIRKD (Yang et al., 2022b), a complex distillation method only attains 74.50% mIoU. Note that our baseline is not stronger than theirs: our DL3-R18 trained with CE has $72.47 \pm 0.33\%$ mIoU while their number is 73.21%.

Albeit IoU losses are becoming increasingly popular in medical imaging, we find CE is still frequently used in the literature on natural images. We adopt training recipes that are optimized for CE and yet obtain noticeable improvements with JML. We hope the promising results of integrating soft labels in our work can further raise the community’s attention on adopting JMLs to natural image datasets such as Cityscapes and PASCAL VOC.

3.3. Calibration

Calibration measures the difference between a network’s confidence to its accuracy (Guo et al., 2017) and it is essential for safety-critical applications such as autonomous driving and medical imaging. In addition to improvements on accuracy, soft labels can also reduce models’ over-confidence (Müller et al., 2019; Mobahi et al., 2020; Zhou et al., 2021), thus increasing model calibration. The effects of KD and BLS on calibration are also shown in Tables 1, 2 and 3.

Table 5. Evaluating different losses terms with a DL3-R18 student on Cityscapes and PASCAL VOC. T-JML-BLS means we train the teacher with JML-BLS. S-JML-BLS means we train the student with JML-BLS. All results are mIoU (%).

$\mathcal{L}_{CE, L}$	$\mathcal{L}_{JML, L}$	$\mathcal{L}_{CE, KD}$	$\mathcal{L}_{JML, KD}$	T-JML-BLS	S-JML-BLS	CS (%)	VOC (%)
✓	-	-	-	-	-	72.88 ± 0.44	72.47 ± 0.33
✓	✓	-	-	-	-	75.55 ± 0.13	74.42 ± 0.52
✓	✓	✓	-	-	-	75.74 ± 0.25	74.65 ± 0.42
✓	✓	✓	✓	-	-	76.16 ± 0.37	75.05 ± 0.31
✓	✓	✓	✓	✓	-	76.68 ± 0.33	75.89 ± 0.29
✓	✓	✓	✓	✓	✓	76.21 ± 0.26	75.34 ± 0.31

Table 6. Comparing 3 teachers with different accuracy and calibration on PASCAL VOC.

Metrics	T1	T2	T3
T ECE (%)	4.20	3.47	3.24
T BECE (%)	33.17	20.73	20.42
T mIoU (%)	79.09	78.75	79.82
S ECE (%)	4.76 ± 0.09	4.01 ± 0.07	3.94 ± 0.07
S BECE (%)	33.86 ± 0.10	22.21 ± 0.06	22.15 ± 0.05
S mIoU (%)	75.05 ± 0.31	75.43 ± 0.35	75.89 ± 0.29

Table 7. Comparing different modes to compute active classes on PASCAL VOC with DL3-R18. All results are mIoU (%).

Method	all	present	label	prob	both
JML-BLS	75.60 ± 0.24	74.57 ± 0.51	75.60 ± 0.24	75.22 ± 0.30	75.07 ± 0.18
JML-KD	75.21 ± 0.33	74.50 ± 0.25	75.89 ± 0.29	75.51 ± 0.53	75.39 ± 0.31

As opposed to the common belief in classification, when the model is trained only with CE, we find that both BLS and KD can sometimes deteriorate model calibration. For instance, in Cityscapes experiments, the lowest ECE and SCE is usually obtained with CE. Nevertheless, CE-BLS can still improve model calibration near the boundary region.

Although the soft Dice loss can significantly increase a model’s segmentation performance, it can hurt model calibration (Mehrtash et al., 2020; Bertels et al., 2021). We confirm that this is also the case for JML. However, we can mitigate this issue by training the model with soft labels. For JML experiments, both JML-BLS and JML-KD reliably increase model calibration. One can further increase model calibration with post-hoc (Guo et al., 2017; Ding et al., 2021; Ma & Blaschko, 2021; Popordanoska et al., 2021; Rousseau et al., 2021) and trainable calibration methods (Kumar et al., 2018; Popordanoska et al., 2022), which is out of the scope of this paper.

4. Ablation Studies

4.1. Boundary Label Smoothing

BLS is sensitive to the choice of ϵ . Effects of ϵ with DL3-R101, DL3-R50 and DL3-R18 on PASCAL VOC are shown in Figure 5 (in the appendix). Being simple and cheap, BLS can effectively increase model accuracy and calibration. Interestingly, for DL3-R50 and DL3-R18, the optimal ϵ that achieves the highest mIoU is the one with the lowest ECE.

The optimal ϵ for different k of the DL3-R18 is shown in Figure 6 (in the appendix). Note that $k = \infty$ means we apply LS to every pixel. Generally, as k increases, we need to decrease the strength of smoothing. We find the best result is obtained when $k = 3$ and $\epsilon = 0.50$.

4.2. Knowledge Distillation

We examine the contribution of each loss term in Table 5. Adding JML terms can greatly improve the performance of the student.

In classification, it is observed that the teacher trained with LS could hurt the performance of the student (Müller et al., 2019). This is often presented as an counterexample that a more accurate teacher may not distill a better student. However, we find that the student benefits from the teacher trained with JML-BLS. We believe the teacher learns intricate boundary information through JML-BLS, and this dark knowledge is implicitly passed to the student, thus leading to a more accurate student. However, if we also train the student with JML-BLS, the accuracy will drop. Thus, it is more effectively for the student to learn this boundary information from the teacher rather than from the label.

What exactly is this boundary information? We believe it relates to the calibration of the teacher. The student with less capacity often struggles to mimic a powerful teacher, especially near ambiguous boundary regions. However, if the teacher is more calibrated and outputs a less peaked

distribution, the student will learn this uncertainty rather than trying to match an unrealistic distribution that it does not have enough capacity to reproduce.

In Table 6, we compare three teachers with different accuracy and calibration on PASCAL VOC. Both T2 and T3 are trained with JML-BLS, while T1 is not. T2 has a lower mIoU than T1 but is more calibrated. As a result, T2’s student is more accurate and calibrated than T1’s.

4.3. Active Classes

We study the impact of active classes on PASCAL VOC in Table 7. Note that for JML-BLS, depending on the magnitude of the threshold, mode “label” is identical to either “all” or “present”.

Choosing active classes is important. Looking at “all” classes in JML-KD can distract the student. In most of the teacher’s output classes, the confidence is usually a very small number. It can be difficult for the student to reproduce these meaningless numbers. With mode “present”, the performance is similar to without soft labels. It is because the power of soft labels depends on non-argmax classes. “prob” and “both” achieve similar performance, but both are worse than “label”. In our experiments, the best results in both JML-BLS and JML-KD are obtained with “label” where at each iteration, the model will only look at the most significant classes.

5. Related Works

5.1. IoU Losses

IoU is a commonly used metric in semantic segmentation and IoU losses aim at directly optimizing this metric. IoU only obtains values when both predictions and ground-truth labels are discrete binary vectors $\{0, 1\}^p$, but the neural network often predicts soft probabilities (after the softmax or sigmoid layer) in $[0, 1]^p$. In order to interpolate values of IoU from $\{0, 1\}^p$ to $[0, 1]^p$, currently there are two popular directions. The one is to relax set counting as norm functions, such as the soft Jaccard loss (Nowozin, 2014; Rahman & Wang, 2016), the soft Dice loss (Sudre et al., 2017), the soft Tversky loss (Salehi et al., 2017) and the focal Tversky loss (Abraham & Khan, 2019). The other is based on the fact that IoU is submodular (Yu & Blaschko, 2018), so the convex Lovasz extension of submodular functions can be applied. For instance, the Lovasz-Softmax loss (Berman et al., 2018), the Lovasz hinge loss (Yu & Blaschko, 2018) and the PixIoU loss (Yu et al., 2021). Nevertheless, as one extends the value of IoU for predictions from $\{0, 1\}^p$ to $[0, 1]^p$, the fact that labels can also be in $[0, 1]^p$ is overlooked. As a result, these IoU losses are incompatible with soft labels.

IoU is adopted in a wide range of fields and due to its dis-

crete nature, its probabilistic extensions (Späth, 1981) have also been considered in object detection (Feng et al., 2022), medical imaging (Dorent et al., 2020) and information retrieval (Ioffe, 2010; Moulton & Jiang, 2018).

5.2. Soft Labels

Soft labels are pervasive in machine learning. For example, in data augmentation techniques such as MixUp (Zhang et al., 2018) and CutMix (Yun et al., 2019), two hard labels are mixed to generate a single soft label. In label smoothing (Szegedy et al., 2016), soft labels are produced via a weighted average of hard labels and the uniform distribution over labels. In knowledge distillation (Hinton et al., 2015), a student model needs to match a teacher’s soft predictions. Knowledge distillation is mostly used in model compression (Hinton et al., 2015; Liu et al., 2019), but it is also adopted in many other areas such as adversarial machine learning (Papernot et al., 2016), self-training or self-distillation (Xie et al., 2020; Yang et al., 2022a), dynamic inference (Yu & Huang, 2019; Yu et al., 2019) and neural architecture search (Berman et al., 2020; Li et al., 2020). In particular, label smoothing and knowledge distillation have been employed in many state-of-the-art models and shown to improve both network’s accuracy and calibration (Müller et al., 2019). Soft labels are also found in other fields such as partial label learning (Wang et al., 2022) and semi-supervised learning (Laine & Aila, 2017; Berthelot et al., 2019; Liu et al., 2022).

6. Conclusion

In this paper, we propose Jaccard metric losses (JMLs), which are variants of the soft Jaccard loss so as to make it compatible with soft labels. We study two of the most popular use cases of soft labels: label smoothing and knowledge distillation. In order to optimize the model with JMLs in these settings, we investigate different modes to compute active classes. We conduct extensive experiments on Cityscapes, PASCAL VOC and DeepGlobe Land. In particular, our simple approach JML-KD that only utilizes soft labels, exceeds state-of-the-arts knowledge distillation methods by a large margin on various datasets and architectures.

Acknowledgements

We acknowledge support from the Research Foundation - Flanders (FWO) through project numbers G0A1319N and S001421N, and funding from the Flemish Government under the Onderzoeksprogramma Artificiële Intelligentie (AI) Vlaanderen programme. The resources and services used in this work were provided by the VSC (Flemish Supercomputer Center), funded by the Research Foundation - Flanders (FWO) and the Flemish Government.

References

- Abraham, N. and Khan, N. M. A Novel Focal Tversky Loss Function with Improved Attention U-Net for Lesion Segmentation. *ISBI*, 2019.
- Berman, M., Triki, A. R., and Blaschko, M. B. The Lovasz-softmax loss: A Tractable Surrogate for the Optimization of the Intersection-Over-Union Measure in Neural Networks. *CVPR*, 2018.
- Berman, M., Pishchulin, L., Xu, N., Blaschko, M., and Medioni, G. AOWS: Adaptive and Optimal Network Width Search with Latency Constraints. *CVPR*, 2020.
- Bertels, J., Robben, D., Vandermeulen, D., and Suetens, P. Theoretical analysis and experimental validation of volume bias of soft Dice optimized segmentation maps in the context of inherent uncertainty. *MIA*, 2021.
- Berthelot, D., Carlini, N., Goodfellow, I., Papernot, N., Oliver, A., and Raffel, C. MixMatch: A Holistic Approach to Semi-Supervised Learning. *NeurIPS*, 2019.
- Chen, L.-C., Papandreou, G., Schroff, F., and Adam, H. Rethinking Atrous convolution for semantic image segmentation. *arXiv*, 2017.
- Cordts, M., Omran, M., Ramos, S., Rehfeld, T., Enzweiler, M., Benenson, R., Franke, U., Roth, S., and Schiele, B. The Cityscapes Dataset for Semantic Urban Scene Understanding. *CVPR*, 2016.
- Demir, I., Koperski, K., Lindenbaum, D., Pang, G., Huang, J., Basu, S., Hughes, F., Tuia, D., and Raskar, R. DeepGlobe 2018: A Challenge to Parse the Earth through Satellite Images. *CVPR Workshop*, 2018.
- Deng, J., Dong, W., Socher, R., Li, L.-J., Li, K., and Fei-Fei, L. ImageNet: A Large-Scale Hierarchical Image Database. *CVPR*, 2009.
- Ding, Z., Han, X., Liu, P., and Niethammer, M. Local Temperature Scaling for Probability Calibration. *ICCV*, 2021.
- Dorent, R., Booth, T., Li, W., Sudre, C. H., Kafiabadi, S., Cardoso, J., Ourselin, S., and Vercauteren, T. Learning joint segmentation of tissues and brain lesions from task-specific hetero-modal domain-shifted datasets. *MIA*, 2020.
- Eelbode, T., Bertels, J., Berman, M., Vandermeulen, D., Maes, F., Bisschops, R., and Blaschko, M. B. Optimization for medical image segmentation: Theory and Practice When Evaluating With Dice Score or Jaccard Index. *TMI*, 2020.
- Everingham, M., Gool, L. V., Williams, C. K. I., Winn, J., and Zisserman, A. The Pascal Visual Object Classes (VOC) Challenge. *IJCV*, 2009.
- Feng, D., Wang, Z., Zhou, Y., Rosenbaum, L., Timm, F., Dietmayer, K., Tomizuka, M., and Zhan, W. Labels are Not Perfect: Inferring Spatial Uncertainty in Object Detection. *TITS*, 2022.
- Guo, C., Pleiss, G., Sun, Y., and Weinberger, K. Q. On calibration of modern neural networks. *ICML*, 2017.
- He, K., Zhang, X., Ren, S., and Sun, J. Deep residual learning for image recognition. *CVPR*, 2016.
- Hinton, G., Vinyals, O., and Dean, J. Distilling the knowledge in a neural network. *NeurIPS Workshop*, 2015.
- Huang, T., You, S., Wang, F., Qian, C., and Xu, C. Knowledge Distillation from A Stronger Teacher. *NeurIPS*, 2022a.
- Huang, T., Zhang, Y., You, S., Wang, F., Qian, C., Cao, J., and Xu, C. Masked Distillation with Receptive Tokens. *arXiv*, 2022b.
- Iakubovskii, P. Segmentation models pytorch. https://github.com/qubvel/segmentation_models.pytorch, 2019.
- Ioffe, S. Improved Consistent Sampling, Weighted Minhash and L1 Sketching. *ICDM*, 2010.
- Isensee, F., Jaeger, P. F., Kohl, S. A. A., Petersen, J., and Maier-Hein, K. H. nnU-Net: a self-configuring method for deep learning-based biomedical image segmentation. *Nature Methods*, 2021.
- Kosub, S. A note on the triangle inequality for the Jaccard distance. *PRL*, 2019.
- Kumar, A., Sarawagi, S., and Jain, U. Trainable Calibration Measures For Neural Networks From Kernel Mean Embeddings. *ICML*, 2018.
- Laine, S. and Aila, T. Temporal Ensembling for Semi-Supervised Learning. *ICLR*, 2017.
- Li, C., Peng, J., Yuan, L., Wang, G., Liang, X., Lin, L., and Chang, X. Block-wisely supervised neural architecture search with knowledge distillation. *CVPR*, 2020.
- Li, H., Tao, C., Zhu, X., Wang, X., Huang, G., and Dai, J. Auto Seg-Loss: Searching Metric Surrogates for Semantic Segmentation. *ICLR*, 2021.
- Li, H., Fu, T., Dai, J., Li, H., Huang, G., and Zhu, X. AutoLoss-Zero: Searching Loss Functions from Scratch for Generic Tasks. *CVPR*, 2022.

- Lin, T.-Y., Goyal, P., Girshick, R., He, K., and Dollár, P. Focal Loss for Dense Object Detection. *TPAMI*, 2018.
- Liu, Y., Chen, K., Liu, C., Qin, Z., Luo, Z., and Wang, J. Structured Knowledge Distillation for Semantic Segmentation. *CVPR*, 2019.
- Liu, Y., Tian, Y., Chen, Y., Liu, F., Belagiannis, V., and Carneiro, G. Perturbed and Strict Mean Teachers for Semi-supervised Semantic Segmentation. *CVPR*, 2022.
- Ma, X. and Blaschko, M. B. Meta-Cal: Well-controlled Post-hoc Calibration by Ranking. *ICML*, 2021.
- Mehrtash, A., Wells, W. M., Tempany, C. M., Abolmaesumi, P., and Kapur, T. Confidence Calibration and Predictive Uncertainty Estimation for Deep Medical Image Segmentation. *TMI*, 2020.
- Mobahi, H., Farajtabar, M., and Bartlett, P. L. Self-Distillation Amplifies Regularization in Hilbert Space. *NeurIPS*, 2020.
- Moulton, R. and Jiang, Y. Maximally Consistent Sampling and the Jaccard Index of Probability Distributions. *ICDM Workshop*, 2018.
- Müller, R., Kornblith, S., and Hinton, G. When Does Label Smoothing Help? *NeurIPS*, 2019.
- Nowozin, S. Optimal Decisions from Probabilistic Models: the Intersection-over-Union Case. *CVPR*, 2014.
- Papernot, N., McDaniel, P., Wu, X., Jha, S., and Swami, A. Distillation as a Defense to Adversarial Perturbations Against Deep Neural Networks. *S&P*, 2016.
- Popordanoska, T., Bertels, J., Vandermeulen, D., Maes, F., and Blaschko, M. B. On the relationship between calibrated predictors and unbiased volume estimation. *MICCAI*, 2021.
- Popordanoska, T., Sayer, R., and Blaschko, M. B. A Consistent and Differentiable Lp Canonical Calibration Error Estimator. *NeurIPS*, 2022.
- Rahman, M. A. and Wang, Y. Optimizing intersection-over-union in deep neural networks for image segmentation. *ISVC*, 2016.
- Rakhlina, A., Davydov, A., and Nikolenko, S. Land Cover Classification from Satellite Imagery With U-Net and Lovász-Softmax Loss. *CVPR Workshop*, 2018.
- Ronneberger, O., Fischer, P., and Brox, T. U-Net: Convolutional Networks for Biomedical Image Segmentation. *MICCAI*, 2015.
- Rousseau, A.-J., Becker, T., Bertels, J., Blaschko, M. B., and Valkenburg, D. Post training uncertainty calibration of deep networks for medical image segmentation. *ISBI*, 2021. doi: PostRousseauISBI2021.
- Salehi, S. S. M., Erdogmus, D., and Gholipour, A. Tversky loss function for image segmentation using 3D fully convolutional deep networks. *MICCAI Workshop*, 2017.
- Sandler, M., Howard, A., Zhu, M., Zhmoginov, A., and Chen, L.-C. MobileNetV2: Inverted Residuals and Linear Bottlenecks. *CVPR*, 2018.
- Shu, C., Liu, Y., Gao, J., Yan, Z., and Shen, C. Channel-wise Knowledge Distillation for Dense Prediction. *ICCV*, 2021.
- Späth, H. The minisum location problem for the Jaccard metric. *OR Spektrum*, 1981.
- Sudre, C. H., Li, W., Vercauteren, T., Ourselin, S., and Cardoso, M. J. Generalised Dice overlap as a deep learning loss function for highly unbalanced segmentations. *MICCAI Workshop*, 2017.
- Szegedy, C., Vanhoucke, V., Ioffe, S., Shlens, J., and Wojna, Z. Rethinking the Inception Architecture for Computer Vision. *CVPR*, 2016.
- Tang, J., Shivanna, R., Zhao, Z., Lin, D., Singh, A., Chi, E. H., and Jain, S. Understanding and Improving Knowledge Distillation. *arXiv*, 2020.
- Vapnik, V. N. *The Nature of Statistical Learning Theory*. Springer, 1995.
- Wang, H., Xiao, R., Li, Y., Feng, L., Niu, G., Chen, G., and Zhao, J. PiCO: Contrastive Label Disambiguation for Partial Label Learning. *ICLR*, 2022.
- Wang, Y., Zhou, W., Jiang, T., Bai, X., and Xu, Y. Intra-class Feature Variation Distillation for Semantic Segmentation. *ECCV*, 2020.
- Wightman, R. Pytorch image models. <https://github.com/rwightman/pytorch-image-models>, 2019.
- Xie, Q., Luong, M.-T., Hovy, E., and Le, Q. V. Self-training with noisy student improves ImageNet classification. *CVPR*, 2020.
- Yang, C., An, Z., Zhou, H., Cai, L., Zhi, X., Wu, J., Xu, Y., and Zhang, Q. MixSKD: Self-Knowledge Distillation from Mixup for Image Recognition. *ECCV*, 2022a.
- Yang, C., Zhou, H., An, Z., Jiang, X., Xu, Y., and Zhang, Q. Cross-Image Relational Knowledge Distillation for Semantic Segmentation. *CVPR*, 2022b.

- Yu, J. and Blaschko, M. B. The Lovász Hinge: A Novel Convex Surrogate for Submodular Losses. *TPAMI*, 2018.
- Yu, J. and Huang, T. S. Universally slimmable networks and improved training techniques. *ICCV*, 2019.
- Yu, J., Yang, L., Xu, N., Yang, J., and Huang, T. Slimmable neural networks. *ICLR*, 2019.
- Yu, J., Xu, J., Chen, Y., Li, W., Wang, Q., Yoo, B. I., and Han, J.-J. Learning generalized intersection over union for dense pixelwise prediction. *ICML*, 2021.
- Yuan, L., Tay, F. E., Li, G., Wang, T., and Feng, J. Revisiting Knowledge Distillation via Label Smoothing Regularization. *CVPR*, 2020.
- Yun, S., Han, D., Oh, S. J., Chun, S., Choe, J., and Yoo, Y. CutMix: Regularization Strategy to Train Strong Classifiers with Localizable Features. *ICCV*, 2019.
- Zhang, H., Cisse, M., Dauphin, Y. N., and Lopez-Paz, D. mixup: Beyond Empirical Risk Minimization. *ICLR*, 2018.
- Zhao, B., Cui, Q., Song, R., Qiu, Y., and Liang, J. Decoupled Knowledge Distillation. *CVPR*, 2022.
- Zhao, H., Shi, J., Qi, X., Wang, X., and Jia, J. Pyramid Scene Parsing Network. *CVPR*, 2017.
- Zhou, H., Song, L., Chen, J., Zhou, Y., Wang, G., Yuan, J., and Zhang, Q. Rethinking Soft Labels for Knowledge Distillation: A Bias-Variance Tradeoff Perspective. *ICLR*, 2021.

A. The Lovasz-Softmax Loss

Based on the fact that IoU is submodular (Yu & Blaschko, 2018), the Lovasz-Softmax loss (Berman et al., 2018) computes the convex Lovasz extension of IoU. Specifically, for each prediction $x_i \in [0, 1]$, mispredictions are computed as:

$$m_i = \begin{cases} 1 - x_i & \text{if } y_i = 1, \\ x_i & \text{otherwise.} \end{cases} \quad (18)$$

The Lovasz extension can be applied such that

$$\begin{aligned} \bar{\Delta}_{\text{LSL}} : m \in [0, 1]^p, y \in \{0, 1\}^p \\ \mapsto \sum_{i=1}^p m_i g_i(m) \end{aligned} \quad (19)$$

where $g_i(m) = \Delta_{\text{IoU}}(\{\pi_1, \dots, \pi_i\}) - \Delta_{\text{IoU}}(\{\pi_1, \dots, \pi_{i-1}\})$ and π is a permutation ordering of m such that $m_{\pi_1} \geq \dots \geq m_{\pi_p}$.

Loss functions that rely on the Lovasz extension, such as the Lovasz-Softmax loss (Berman et al., 2018), the Lovasz hinge loss (Yu & Blaschko, 2018) and the PixIoU loss (Yu et al., 2021) cannot handle soft labels because they need to compute $g_i(m)$ and it requires $y \in \{0, 1\}^p$.

B. Proof of Theorem 2.2

Proof. (i) $\bar{\Delta}_{\text{JML},1}$ is a metric in $[0, 1]^p$. The proof was given in (Späth, 1981). Here we provide a sketch for the proof of the triangle inequality.

$$\bar{\Delta}_{\text{JML},1} = 1 - \frac{\|x\|_1 + \|y\|_1 - \|x - y\|_1}{\|x\|_1 + \|y\|_1 + \|x - y\|_1} \quad (20)$$

$$= \frac{2\|x - y\|_1}{\|x\|_1 + \|y\|_1 + \|x - y\|_1}. \quad (21)$$

Given a fixed point $a \in [0, 1]^p$, the key is to define a new function d' :

$$d'(x, y) = \begin{cases} 0 & \text{if } x = y = a, \\ \frac{d(x, y)}{d(x, a) + d(y, a) + d(x, y)} & \text{otherwise;} \end{cases} \quad (22)$$

and show that if d is a metric in $[0, 1]^p$, then d' is also a metric in $[0, 1]^p$. Given that L^1 norm is a metric in $[0, 1]^p$, we can conclude that $\bar{\Delta}_{\text{JML},1}$ is also a metric in $[0, 1]^p$.

(ii) $\bar{\Delta}_{\text{JML},2}$ is a metric in $[0, 1]^p$. Conditions (i) - (iii) are

obvious. To show the triangle inequality, note that

$$\|b \odot c\|_1 = \sum_i b_i c_i \quad (23)$$

$$= \sum_i ((b_i - a_i)c_i + a_i c_i) \quad (24)$$

$$\leq \sum_i |b_i - a_i| + \sum_i a_i c_i \quad (25)$$

$$= \|a - b\|_1 + \|a \odot c\|_1. \quad (26)$$

Similarly,

$$\|a \odot b\|_1 \leq \|b - c\|_1 + \|a \odot c\|_1. \quad (27)$$

Hence

$$\bar{\Delta}_{\text{JML},2}(a, b) + \bar{\Delta}_{\text{JML},2}(b, c) \quad (28)$$

$$= \frac{\|a - b\|_1}{\|a - b\|_1 + \|a \odot b\|_1} + \frac{\|b - c\|_1}{\|b - c\|_1 + \|b \odot c\|_1} \quad (29)$$

$$\begin{aligned} &\geq \frac{\|a - b\|_1}{\|a - b\|_1 + \|b - c\|_1 + \|a \odot c\|_1} \\ &+ \frac{\|b - c\|_1}{\|a - b\|_1 + \|b - c\|_1 + \|a \odot c\|_1} \end{aligned} \quad (30)$$

$$= \frac{\|a - b\|_1 + \|b - c\|_1}{\|a - b\|_1 + \|b - c\|_1 + \|a \odot c\|_1} \quad (31)$$

$$\geq \frac{\|a - c\|_1}{\|a - c\|_1 + \|a \odot c\|_1} \quad (32)$$

$$= \bar{\Delta}_{\text{JML},2}(a, c) \quad (33)$$

where the last inequality follows from $\|a - b\|_1 + \|b - c\|_1 \geq \|a - c\|_1$.

(iii) $\bar{\Delta}_{\text{SJL},L^1}$ is not a metric in $[0, 1]^p$. For instance, if $a = 0.5$, $\bar{\Delta}_{\text{SJL},L^1}(a, a) = 2/3 \neq 0$.

(iv) $\bar{\Delta}_{\text{SJL},L^2}$ is not a metric in $[0, 1]^p$. For instance, if $a = 0.8$, $b = 0.4$, $c = 0.2$, it does not satisfy the triangle inequality. □

C. Proof of Theorem 2.3

Proof. (i) $\forall x \in [0, 1]^p$, $y \in \{0, 1\}^p$ and $x \in \{0, 1\}^p$, $y \in [0, 1]^p$, $\bar{\Delta}_{\text{SJL},L^1} = \bar{\Delta}_{\text{JML},1} = \bar{\Delta}_{\text{JML},2}$. Due to symmetry, we only need to show the case

$\forall x \in [0, 1]^p, y \in \{0, 1\}^p$. Note that

$$\|x\|_1 = \sum_i x_i = \sum_i \mathbb{1}_{(y_i=0)}x_i + \sum_i \mathbb{1}_{(y_i=1)}x_i \quad (34)$$

$$\|y\|_1 = \sum_i y_i = \sum_i \mathbb{1}_{(y_i=1)} \quad (35)$$

$$\langle x, y \rangle = \|x \odot y\|_1 = \sum_i x_i y_i = \sum_i \mathbb{1}_{(y_i=1)}x_i \quad (36)$$

$$\|x - y\|_1 = \sum_i |x_i - y_i| \quad (37)$$

$$= \sum_i \mathbb{1}_{(y_i=0)}x_i - \sum_i \mathbb{1}_{(y_i=1)}x_i + \sum_i \mathbb{1}_{(y_i=1)}. \quad (38)$$

Thus

$$\bar{\Delta}_{\text{SJL}, L^1} = \bar{\Delta}_{\text{JML}, 1} = \bar{\Delta}_{\text{JML}, 2} \quad (39)$$

$$= \frac{\sum_i \mathbb{1}_{(y_i=1)}x_i}{\sum_i \mathbb{1}_{(y_i=0)}x_i + \sum_i \mathbb{1}_{(y_i=1)}}. \quad (40)$$

(ii) $\exists x, y \in [0, 1]^p, \bar{\Delta}_{\text{SJL}, L^1} \neq \bar{\Delta}_{\text{JML}, 1} \neq \bar{\Delta}_{\text{JML}, 2}$. For instance, if $x = 0.8, y = 0.5, \bar{\Delta}_{\text{SJL}, L^1} \neq \bar{\Delta}_{\text{JML}, 1} \neq \bar{\Delta}_{\text{JML}, 2}$

□

D. $\bar{\Delta}_{\text{JML}, 1}$ vs. $\bar{\Delta}_{\text{JML}, 2}$

Definition D.1 (Convex Closure). The convex closure of a set function $f : x \in \{0, 1\}^p \rightarrow [0, 1]$ is defined as

$$\mathcal{C}f : [0, 1]^p \rightarrow [0, 1] = \min_{\alpha} \sum_{i=1}^p \alpha_i f(x_i), \quad (41)$$

$$\text{s.t. } \alpha_i \geq 0, \sum_{i=1}^p \alpha_i = 1, \sum_{i=1}^p \alpha_i x_i = x. \quad (42)$$

The convex closure extends a set function that is only defined at the vertices $\{0, 1\}^p$ to the whole hypercube $[0, 1]^p$ by linearly interpolating the values at these vertices. We plot the loss value of $\bar{\Delta}_{\text{JML}, 1}, \bar{\Delta}_{\text{JML}, 2}$ and the convex closure of $\bar{\Delta}_{\text{SJL}, L^1}$ in Figure 2 when $y = 0.5$. Note that $\bar{\Delta}_{\text{JML}, 1}$ overlaps with the convex closure at $[0, 0.5]$. We can see that $\bar{\Delta}_{\text{JML}, 1} \leq \bar{\Delta}_{\text{JML}, 2}$ and $\bar{\Delta}_{\text{JML}, 1}$ is closer to the convex closure. Generally, we have

Theorem D.2. $\forall x, y \in [0, 1]^p, \bar{\Delta}_{\text{JML}, 1} \leq \bar{\Delta}_{\text{JML}, 2}$.

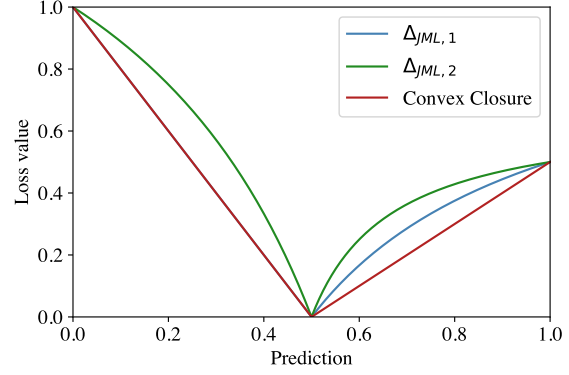


Figure 2. Comparing $\bar{\Delta}_{\text{JML}, 1}, \bar{\Delta}_{\text{JML}, 2}$ and the convex closure with $y = 0.5$.

Proof.

$$\bar{\Delta}_{\text{JML}, 1} \leq \bar{\Delta}_{\text{JML}, 2} \quad (43)$$

$$\Rightarrow \frac{\|x\|_1 + \|y\|_1 - \|x - y\|_1}{\|x\|_1 + \|y\|_1 + \|x - y\|_1}$$

$$- \frac{\|x \odot y\|_1}{\|x \odot y\|_1 + \|x - y\|_1} \geq 0 \quad (44)$$

$$\Rightarrow (\|x\|_1 + \|y\|_1)\|x - y\|_1$$

$$- \|x - y\|_1^2 - 2\|x \odot y\|_1\|x - y\|_1 \geq 0. \quad (45)$$

We can switch the element of x and y whenever $x_i \leq y_i$ for some i . Doing this, each term in the last inequality remains the same. Let us denote the new variable as x', y' such that $x'_i \geq y'_i$ for all i . Hence

$$(\|x\|_1 + \|y\|_1)\|x - y\|_1 - \|x - y\|_1^2 - 2\|x \odot y\|_1\|x - y\|_1 \quad (46)$$

$$= (\|x'\|_1 + \|y'\|_1)\|x' - y'\|_1$$

$$- \|x' - y'\|_1^2 - 2\|x' \odot y'\|_1\|x' - y'\|_1 \quad (47)$$

$$= (\|x'\|_1 + \|y'\|_1)(\|x'\|_1 - \|y'\|_1)$$

$$- (\|x'\|_1 - \|y'\|_1)^2 - 2\|x' \odot y'\|_1(\|x'\|_1 - \|y'\|_1) \quad (48)$$

$$= 2(\|x'\|_1 - \|y'\|_1)(\|y'\|_1 - \|x' \odot y'\|_1) \quad (49)$$

$$= 2 \sum_i (x'_i - y'_i) \sum_i (1 - x'_i)y'_i \geq 0. \quad (50)$$

□

Theorem D.3. Given a set function $l : \{0, 1\}^p \rightarrow [0, 1]$ and two concave functions $f, g : [0, 1]^p \rightarrow [0, 1]$. If $\forall x \in \{0, 1\}^p, l(x) = f(x) = g(x)$ and $\forall x \in [0, 1]^p, f(x) \leq g(x)$, then $\forall x \in [0, 1]^p, |f(x) - \mathcal{C}l(x)| \leq |g(x) - \mathcal{C}l(x)|$.

Proof. It suffices to show $\forall x \in [0, 1]^p, f(x) \geq \mathcal{C}l(x)$.

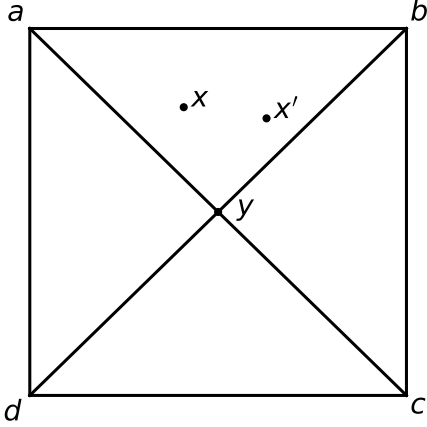


Figure 3. A counterexample that both $\bar{\Delta}_{\text{JML},1}$ and $\bar{\Delta}_{\text{JML},2}$ are not piece-wise concave in 2D.

$\forall x \in [0, 1]^p$, we have $x = \sum_{i=1}^p \alpha_i x_i$ such that $\alpha_i \geq 0$, $\sum_{i=1}^p \alpha_i = 1$ and $x_i \in \{0, 1\}$. Therefore

$$f(x) = f\left(\sum_{i=1}^p \alpha_i x_i\right) \quad (51)$$

$$= f\left((1 - \alpha_p) \frac{\sum_{i=1}^{p-1} \alpha_i x_i}{1 - \alpha_p} + \alpha_p x_p\right) \quad (52)$$

$$\geq (1 - \alpha_p) f\left(\frac{\sum_{i=1}^{p-1} \alpha_i x_i}{1 - \alpha_p}\right) + \alpha_p f(x_p) \quad (53)$$

$$= (1 - \alpha_p) f\left(\frac{1 - \alpha_p - \alpha_{p-1}}{1 - \alpha_p} \frac{\sum_{i=1}^{p-2} \alpha_i x_i}{1 - \alpha_p - \alpha_{p-1}} + \frac{\alpha_{p-1}}{1 - \alpha_p} x_{p-1}\right) + \alpha_p f(x_p) \quad (54)$$

$$\geq (1 - \alpha_p - \alpha_{p-1}) f\left(\frac{\sum_{i=1}^{p-2} \alpha_i x_i}{1 - \alpha_p - \alpha_{p-1}}\right) + \alpha_{p-1} f(x_{p-1}) + \alpha_p f(x_p) \quad (55)$$

$$\geq \dots \geq \sum_{i=1}^p \alpha_i f(x_i) = \sum_{i=1}^p \alpha_i l(x_i) \quad (56)$$

$$\geq \mathcal{C}l(x). \quad (57)$$

□

Although both $\bar{\Delta}_{\text{JML},1}$ and $\bar{\Delta}_{\text{JML},2}$ are not concave as Figure 2 shows, if we can divide the hypercube into several sub-spaces such that $\bar{\Delta}_{\text{JML},1}$ and $\bar{\Delta}_{\text{JML},2}$ are equal at the vertices and concave at each sub-space, then we can still apply Theorem D.3. However, the fact that both of them are piece-wise concave in 1D does not hold in higher dimension. Indeed,

we can find a counterexample in 2D. Let $y = [0.5, 0.5]$, $x = [0.4087, 0.7855]$, $x' = [0.6285, 0.7551]$. Both x and x' are in the sub-space yab and

$$0.5\bar{\Delta}_{\text{JML},1}(x, y) + 0.5\bar{\Delta}_{\text{JML},1}(x', y) > \bar{\Delta}_{\text{JML},1}(0.5x + 0.5x', y), \quad (58)$$

$$0.5\bar{\Delta}_{\text{JML},2}(x, y) + 0.5\bar{\Delta}_{\text{JML},2}(x', y) > \bar{\Delta}_{\text{JML},2}(0.5x + 0.5x', y). \quad (59)$$

How do they perform empirically? In Table 8, we compare $\bar{\Delta}_{\text{JML},1}$ and $\bar{\Delta}_{\text{JML},2}$ on Cityscapes and PASCAL VOC with DL3-R18. We find $\bar{\Delta}_{\text{JML},1}$ is slightly better than $\bar{\Delta}_{\text{JML},2}$.

E. More Analysis of $\bar{\Delta}_{\text{SJL},L^1}$

For $x, y \in [0, 1]^p$, let us rewrite $\bar{\Delta}_{\text{SJL},L^1}$ for a particular pixel i :

$$\bar{\Delta}_{\text{SJL},L^1} = 1 - \frac{x_i y_i + b}{x_i + y_i - x_i y_i + a} \quad (60)$$

such that

$$a = \sum_{j \neq i} x_j + \sum_{j \neq i} y_j - \sum_{j \neq i} x_j y_j, \quad (61)$$

$$b = \sum_{j \neq i} x_j y_j. \quad (62)$$

Assume $ab \neq 0$ which is the case of interest. Take the derivative with respect to x_i :

$$\frac{d\bar{\Delta}_{\text{SJL},L^1}}{dx_i} = -\frac{y_i^2 + (a+b)y_i - b}{(x_i + y_i - x_i y_i + a)^2}. \quad (63)$$

The numerator has two roots:

$$r_1 = \frac{-(a+b) - \sqrt{(a+b)^2 + 4b}}{2}, \quad (64)$$

$$r_2 = \frac{-(a+b) + \sqrt{(a+b)^2 + 4b}}{2}. \quad (65)$$

It is easy to see that $r_1 \leq 0 \leq r_2 \leq 1$. Therefore we have

$$\frac{d\bar{\Delta}_{\text{SJL},L^1}}{dx_i} \leq 0 \text{ if } y_i \geq r_2; > 0 \text{ otherwise.} \quad (66)$$

That is, $\bar{\Delta}_{\text{SJL},L^1}$ will push x_i towards either 1 if $y_i > r_2$, or 0 if $y_i < r_2$, rather than making it close to y_i . Since the derivative also depends on the predictions of pixels other than i which are not independent from x_i , the exact behavior of $\bar{\Delta}_{\text{SJL},L^1}$ is a complex process. However, the above analysis still provides an insight of how $\bar{\Delta}_{\text{SJL},L^1}$ will behave on soft labels.

In Table 8, we compare SJL and JMLs with DL3-R18 on Cityscapes and PASCAL VOC. Recall that we use a combination of CE and SJL/JML when training the network, and

Table 8. Comparing $\overline{\Delta}_{\text{SIL},L^1}$, $\overline{\Delta}_{\text{JML},1}$ and $\overline{\Delta}_{\text{JML},2}$ with DL3-R18 on Cityscapes and PASCAL VOC. All results are mIoU (%).

Dataset	Loss	Hard	BLS	KD
CS	$\overline{\Delta}_{\text{SIL},L^1}$	75.55 ± 0.13	75.43 ± 0.34	75.72 ± 0.42
	$\overline{\Delta}_{\text{JML},1}$	75.55 ± 0.13	76.26 ± 0.17	76.68 ± 0.33
	$\overline{\Delta}_{\text{JML},2}$	75.55 ± 0.13	76.31 ± 0.23	76.45 ± 0.26
VOC	$\overline{\Delta}_{\text{SIL},L^1}$	74.42 ± 0.52	74.13 ± 0.20	74.24 ± 0.61
	$\overline{\Delta}_{\text{JML},1}$	74.42 ± 0.52	75.60 ± 0.24	75.89 ± 0.29
	$\overline{\Delta}_{\text{JML},2}$	74.42 ± 0.52	75.31 ± 0.31	75.49 ± 0.35

Table 9. Results of BLS with DL3-R50 and KD with DL3-R18 on 5 folds of DeepGlobe Land. All results are mIoU (%).

Method	Loss	0	1	2	3	4	$\mu \pm \sigma$
BLS	CE	67.56	69.82	69.59	67.88	69.46	68.86 ± 0.81
	JML	68.13	70.48	70.60	69.49	69.93	69.73 ± 0.89
	Diff	0.57	0.66	1.01	0.61	1.47	0.86 ± 0.34
KD	CE	64.93	67.47	66.22	66.37	67.00	66.40 ± 0.86
	JML	67.20	67.96	67.50	67.62	67.84	67.62 ± 0.27
	Diff	2.27	0.49	1.28	1.25	0.84	1.22 ± 0.59

CE is compatible with soft labels. However, since $\overline{\Delta}_{\text{SIL},L^1}$ has the effect of pushing predictions towards the vertices rather than being minimized at $x = y$, the network does not benefit or even suffers from soft labels. Indeed, predictions for multiple classes might be pushed to 1 at the same time, which will cause a conflict and make the training process unstable.

F. More Results on DeepGlobe Land

We report the results of BLS with DL3-R50 and KD with DL3-R18 on 5 folds of DeepGlobe Land in Table 9. Since DeepGlobe Land is a relatively small dataset with only 803 images, results on each fold can be very different. However, if we look at the difference between CE and JML, the mean improvement is more than 2 times the standard deviation.

G. Figures

Code to compute active classes with different modes is shown in Figure 4.

On PASCAL VOC, Figure 5 illustrates the effects of ϵ with DL3-R101, DL3-R50 and DL3-R18; Figure 6 shows the best ϵ and mIoU (%) for different k with DL3-R18.

With a DL3-R18 student, Figures 7 and 8 provide qualitative results on Cityscapes and PASCAL VOC, respectively. The student not only becomes more accurate, but also learns the confidence map from the teacher, thus becoming more calibrated.

```
import torch

# prob.shape = soft_label.shape = (N, C, H, W)
def compute_active_classes(
    prob: torch.Tensor,
    soft_label: torch.Tensor,
    mode: str,
    num_classes: int,
    threshold: float
):
    if mode == "all":
        idx = torch.arange(num_classes)
    elif mode == "present":
        idx = torch.argmax(soft_label, dim=1).unique()
    elif mode == "prob":
        idx = torch.amax(prob, dim=(0,2,3)) > threshold
    elif mode == "label":
        idx = torch.amax(soft_label, dim=(0,2,3)) > threshold
    elif mode == "both":
        idx = torch.amax(prob + soft_label, dim=(0,2,3)) > threshold

    active_classes = torch.arange(num_classes)[idx]

    return active_classes
```

Figure 4. Code to compute active classes with different modes.

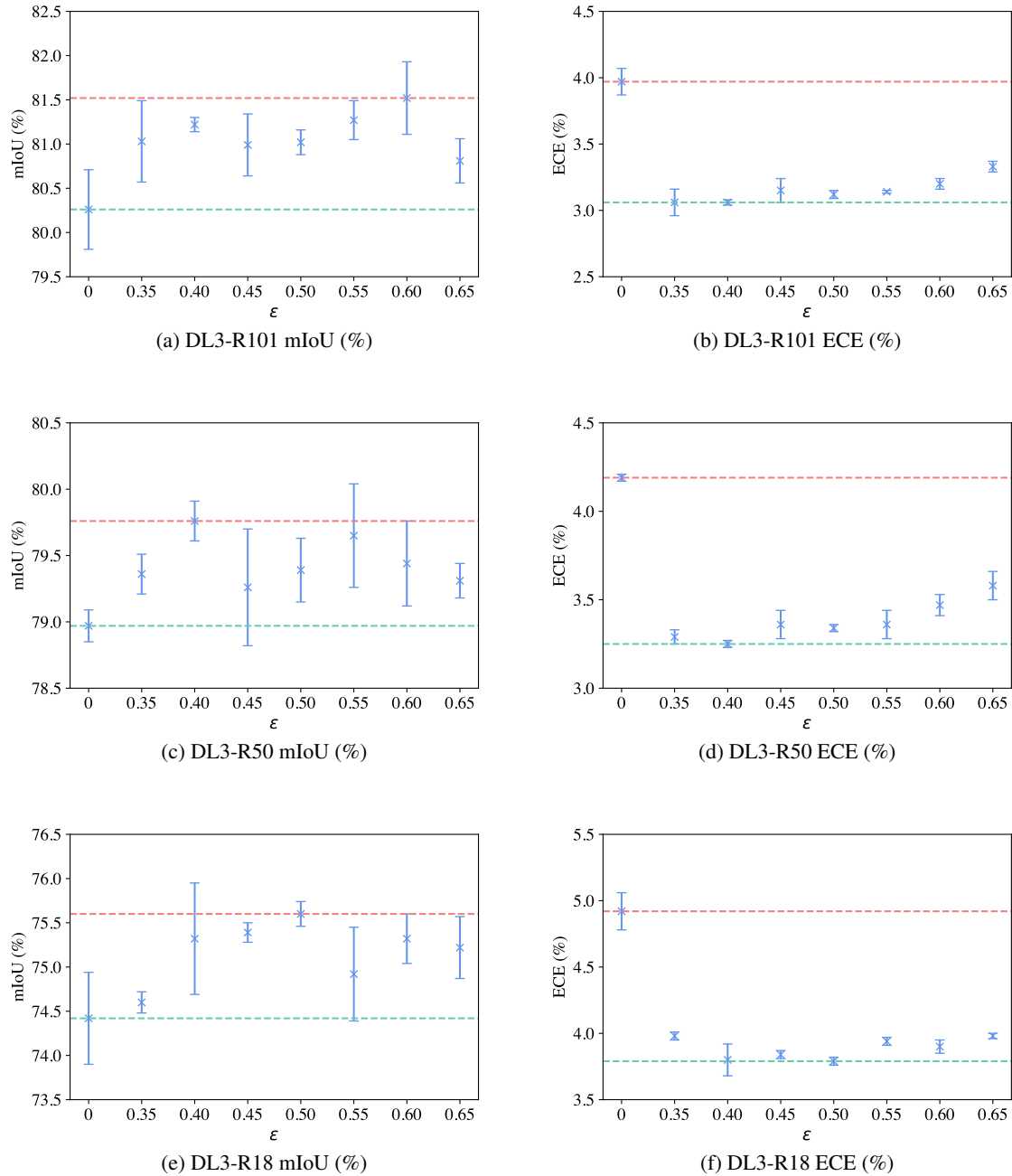


Figure 5. Effects of ϵ with DL3-R101, DL3-R50 and DL3-R18 on PASCAL VOC. $\epsilon = 0$ is the baseline (no smoothing). The highest and the lowest mean values are highlighted in red and green horizontal lines, respectively.

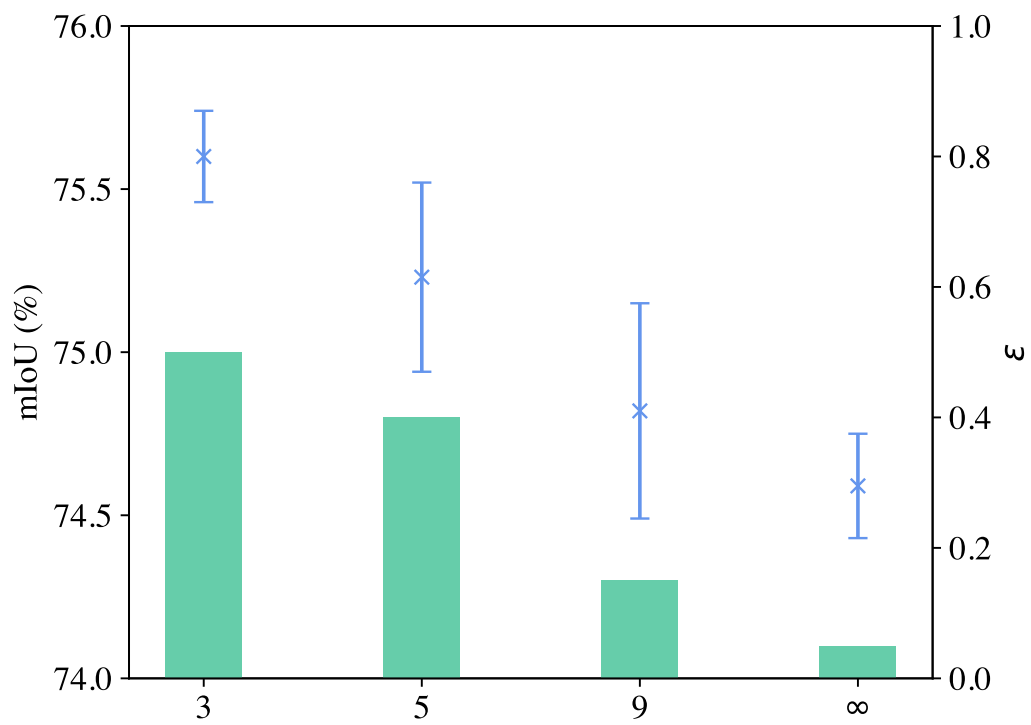


Figure 6. The best ϵ and mIoU (%) for different k with DL3-R18 on PASCAL VOC.

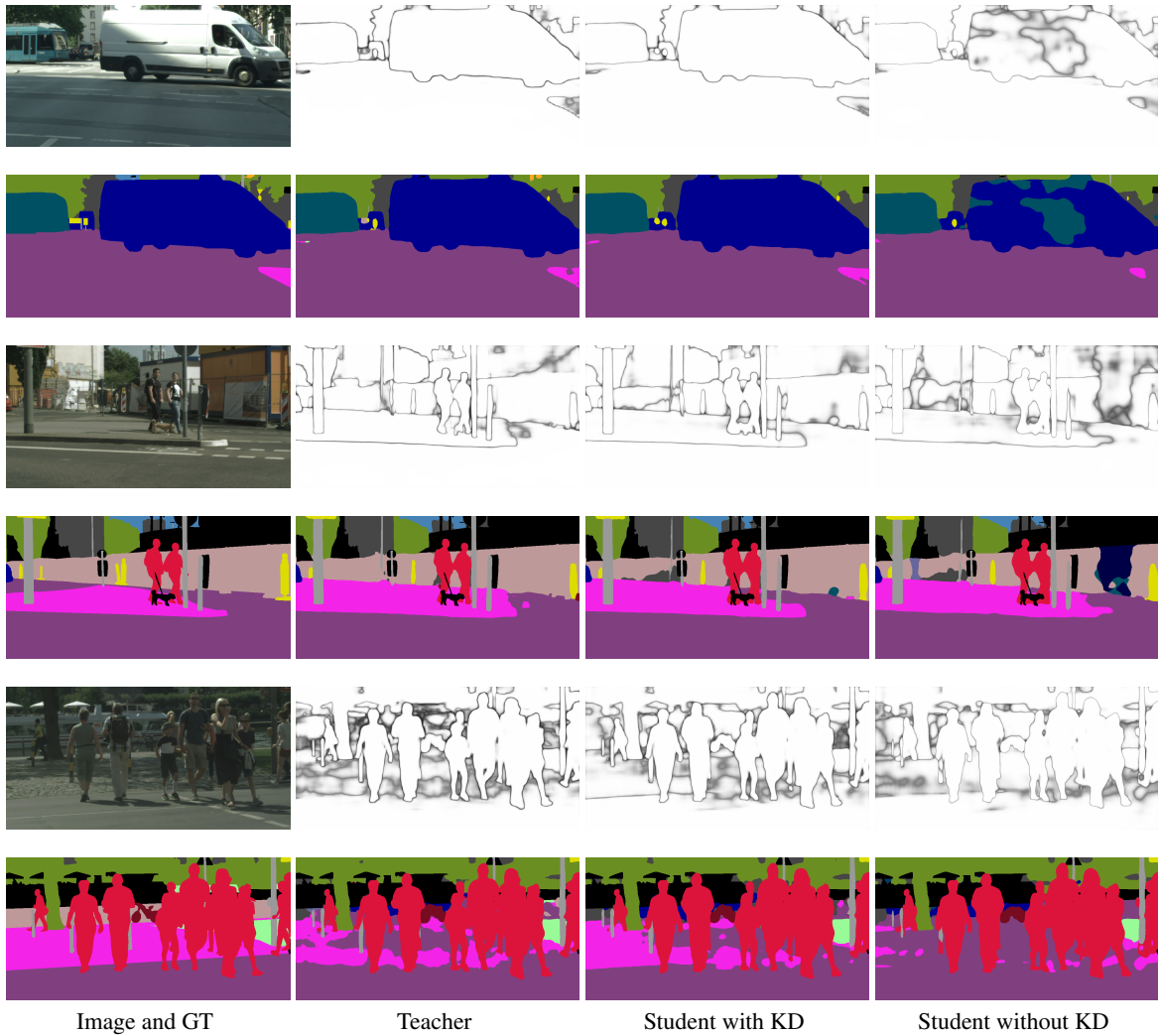


Figure 7. Qualitative results on Cityscapes. Confidence maps are in black and white. Predictions are in RGB.

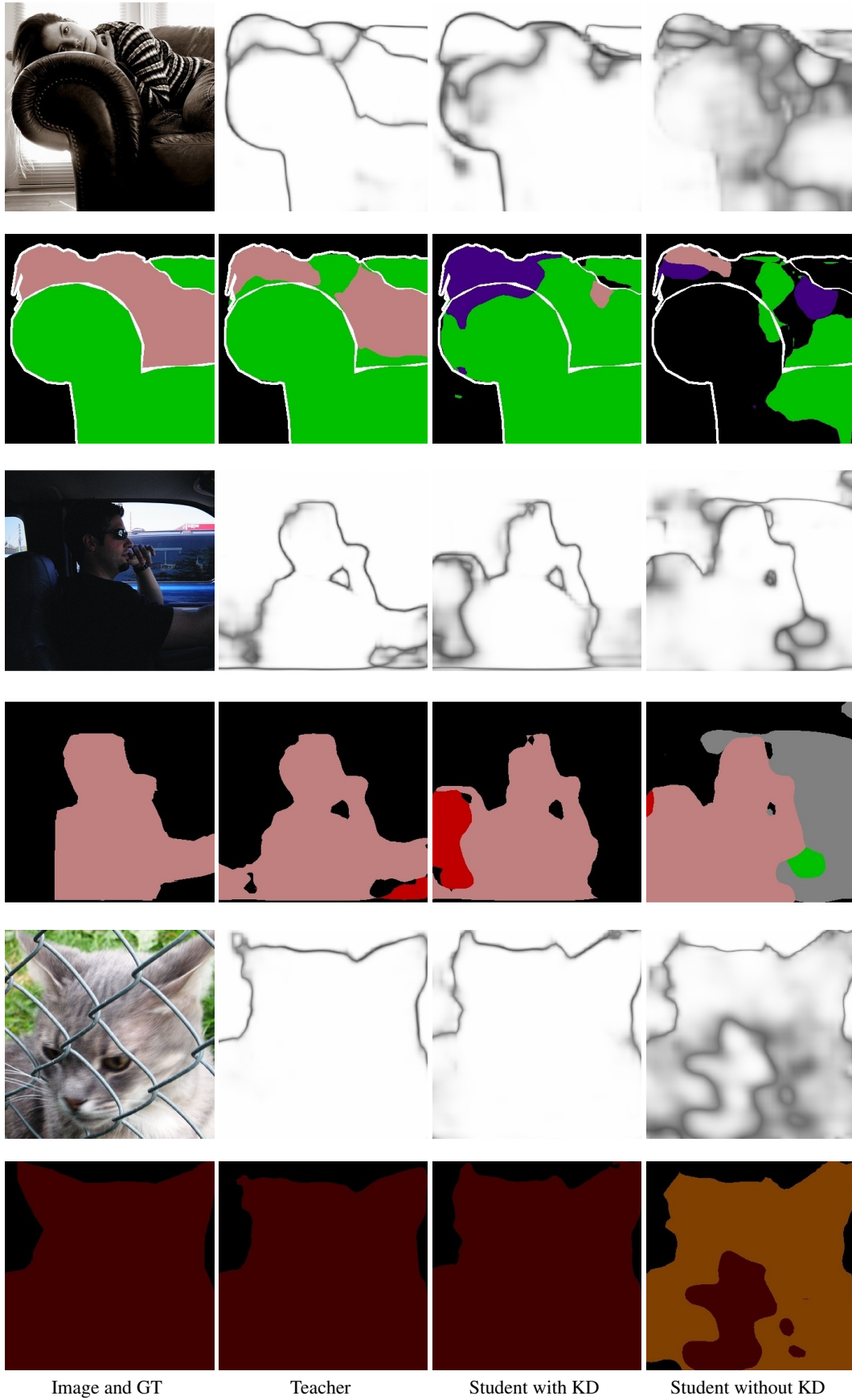


Figure 8. Qualitative results on PASCAL VOC. Confidence maps are in black and white. Predictions are in RGB.